Improving laser-induced breakdown spectroscopy (LIBS) performance for iron and lead determination in aqueous solutions with laser-induced fluorescence (LIF)

Loudyi, Hakim; Rifai, Kheireddine; Laville, Stéphane; Vidal, Francois; Chaker, Mohamed; Sabsabi, Mohamad

Publisher's version / Version de l'éditeur:
https://doi.org/10.1039/B909485G
Journal of Analytical Atomic Spectrometry, 24, 10, pp. 1421-1428, 2009-08-10

Improving laser-induced breakdown spectroscopy (LIBS) performance for iron and lead determination in aqueous solutions with laser-induced fluorescence (LIF)

Hakim Loudyi,[a] Kheireddine Rifaï,[a] Stéphane Laville,[b] François Vidal,*[a] Mohamed Chaker[a] and Mohamad Sabsabi[b]

Received 13th May 2009, Accepted 23rd July 2009
First published as an Advance Article on the web 10th August 2009
DOI: 10.1039/b909485g

The combination of laser-induced breakdown spectroscopy (LIBS) and laser-induced fluorescence (LIF) was investigated to improve the limit of detection (LoD) of trace elements in liquid water, while preserving the distinctive on-line monitoring capabilities of LIBS analysis. The influence of the main experimental parameters, namely the ablation fluence, the excitation fluence, and the inter-pulse delay was studied to maximize the fluorescence signal. The plasma was produced by a 266 nm frequency-quadrupled Q-switched Nd:YAG laser and the trace elements under investigation were then re-excited by a nanosecond optical parametric oscillator (OPO) laser, delivering pulses in the sub-mJ energy range, and tuned to strong absorption lines of the trace elements. The reproducibility of the measurements was improved using a home-made flow-cell, and relative standard deviations as low as 6.7% for a series of 100 shots were attained with a repetition rate of 0.7 Hz. Using the LIBS-LIF technique, we demonstrated LoDs of 39 ppb and 65 ppb for Pb and Fe, respectively, accumulating over 100 laser shots only, which correspond to an improvement of about 500 times with respect to LIBS.

A Introduction

Laser-Induced Breakdown Spectroscopy (LIBS) is an optical diagnostic technique based on emission spectroscopy. It uses a laser beam of moderate power focused onto a material sample (solid, liquid or gas) to generate a luminous plasma. The light emitted by the plasma is then spectrally analyzed to determine the chemical composition of the sample. The main advantages of LIBS over conventional analytical techniques are its ability to analyze samples in situ and remotely with minimal sample preparation. LIBS is already applied in several fields, and its potential applications to the detection of traces elements in liquid samples are of particular interest to the pharmaceutical and mining industries, as well as to environmental monitoring.[1–6]

The major shortcoming of LIBS is clearly its sensitivity, characterized by its limit of detection (LoD), which is generally poorer than for other analytical techniques.[7,8] The value of the LoD obtained by LIBS depends on the element studied and the nature of the sample, and is commonly in the range 1 to 1000 ppm.[9,10] Several approaches have been proposed to improve the analytical performance of the technique regardless the nature of the sample, such as controlling the atmosphere,[11] using two successive laser pulses of arbitrary wavelengths,[12] or different pulse durations,[13–15] among others.[16–20]

In terms of sensitivity, the most promising approach seems to be the LIBS-LIF approach, which combines LIBS with laser-induced fluorescence (LIF). The LIF technique has been studied for decades and demonstrated very high detection efficiency. It has already been associated with several other techniques and reviews on the subject can be found in the literature.[21] The LIBS-LIF approach consists of generating an ablation plasma using a first laser, then re-excite the atoms of the element of interest using a second laser tuned to a specific wavelength, corresponding to a strong absorption line. This hyphenated approach has been studied for the detection of trace elements in solids,[22–30] liquids[31–34] and aerosols,[35] in ambient air or in various controlled atmospheres.

This work aspires to take full advantage of the aforementioned strengths of both techniques to optimize the LoD in the analysis of liquid samples. Although other established techniques can provide a very high sensitivity (down to the ppt-range for Inductively Coupled Plasma – Mass Spectroscopy, for instance[7]), their off-line character prevents them from a universal use. In other words, our main objective here is to preserve the unique in situ, real time capabilities of LIBS analysis, while offering an enhanced trace detection efficiency, well below the ppm-range, thus providing an efficient monitoring device for on-line applications.

Specifically, we applied this technique to measure the concentration of Pb and Fe traces in water-based samples. It is worth stressing that forming suitable laser plasmas for LIBS or LIBS-LIF analysis in liquid samples presents particular challenges due to the generation of waves and bubbles on the liquid surface, splashing of large droplets, and suspension of fine aerosols in the laser beam path that affect the repeatability of the laser-sample interaction. Previous works have been devoted to the reduction of these effects in LIBS measurements, while

[a]*INRS Énergie, Matériaux et Télécommunications, 1650 Boul. Lionel-Boulet, Varennes, Québec, Canada H3C 3J7. E-mail: vidal@emt.inrs.ca; Fax: +1 450 929 8102; Tel: +1 450 929 8118*
[b]*National Research Council of Canada, Industrial Materials Institute, 75 de Mortagne Blvd, Boucherville, Québec, Canada J4B 6Y4*

keeping a reasonable ablation laser repetition rate, including liquid jet systems or strategies involving the evaporation of the liquid samples after deposition on solid substrates.[36,37] In this purpose, we developed a circulation cell providing a constant level of horizontal laminar flow of the liquid, coupled to a system of air circulation, which resulted in a highly reproducible laser-liquid interaction. This shot-to-shot regularity in the LIBS plasma generation (shot-to-shot consistency in the ablated mass) straightforwardly ensured a reproducible overall LIBS-LIF operation.

Minimizing the LoD is in fact equivalent to maximizing the fluorescence signal-to-noise ratio. This requires the excitation beam to be focused in the volume of a laser-induced plasma where optimal conditions prevail, mainly in terms of temperature, atom density and size of the plasma, for a given setup. Since laser-produced plasmas are dynamic media, minimizing the LoD implies the optimization of several experimental parameters, the most important being: (1) the fluence of the ablation laser, (2) the fluence of the excitation laser, and (3) the delay between the two laser pulses. In this work, we studied the dependence of the LIF signal in terms of these parameters and determined an optimum. This optimization process led us to lower the LoD by a factor of about 500 compared to conventional LIBS analysis conducted in the best conditions using the same setup.

B Experimental setup

Our experimental setup is shown in Fig. 1. The ablation was carried out using a 266 nm, frequency-quadrupled Q-switched Nd:YAG laser (Continuum, Surelite II). The pulse width was 7 ns (FWHM) and the maximum output energy at this specific wavelength was about 40 mJ per pulse. The beam was focused onto the surface of the liquid using a plano-convex lens (25.4-mm diameter, 20.6-cm focal length) at normal incidence. The spot diameter onto the liquid surface was about 500 μm. The ablation fluence (F_{ABL}) was varied from a few J/cm^2 to 20 J/cm^2, which corresponds to the maximum available fluence. The repetition rate was set to only 0.7 Hz to avoid problems arising from laser-aerosol interactions and ensure a flat, fresh and reproducible liquid surface. All the measurements were carried out in air at atmospheric pressure.

After formation of the plasma, a second pulse provided by an optical parametric oscillator (OPO) laser (Continuum, Panther) was focused into the plasma by a plano-convex fused silica lens (25.4-mm diameter, 20.6-cm focal length) to re-excite the trace element under investigation. The angle θ between the ablation and the excitation beams was about 10°, and the OPO spot on the plasma, elliptically-shaped, was estimated to be about 1 × 3 mm^2. The OPO laser was pumped by a 355 nm frequency tripled Q-switched Nd:YAG laser with an energy limited to about 250 mJ per pulse. The OPO pulse duration was 7 ns (FWHM) while its repetition rate was 10 Hz (but used in single-shot mode). The wavelength of the OPO laser could be tuned from 215 nm to 2.7 μm and the corresponding energy (E_{OPO}) ranged from 10 μJ (at about 320 nm) to 70 mJ (at about 450 nm). In this work, the OPO energy was varied from a few hundred of nJ to several hundreds of μJ using a set of neutral density filters. This corresponds to a maximum fluence of tens of mJ/cm^2, which is much lower than the ablation threshold of liquid water for nanosecond pulses, estimated from our measurements to a few J/cm^2 for 266 nm laser pulses, and to even higher values from the literature, for 355 nm[38] and for 532 nm[39] pulses. The excitation energy was measured using a low energy pyroelectric detector (Ophir, PE10). The synchronization of the two laser pulses was achieved using an 8-channel programmable delay generator (model 565, Berkeley Nucleonics Corporation).

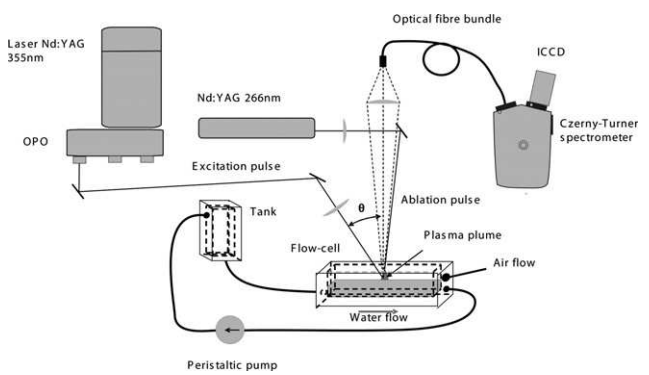

Fig. 1 Schematic of the experimental setup.

The fluorescence signal emitted by the plasma was then collected by a plano-convex lens (50.8 mm-diameter, 10.6-cm focal length) and focused into an optical fibre bundle of 1-mm-total core diameter (the bundle was an assembly of twenty five 100-μm-diameter fibres). The vertically-aligned output of the optical fibre bundle was positioned at the entrance slit of a Czerny-Turner spectrometer (VM 504, Acton Research). The focal length of the spectrometer was 0.39 m while its effective aperture was F/5.4. The spectrometer was equipped with a 1200 lines/mm grating (blazed at 150 nm) or a 2400 lines/mm grating (optimized in the UV-visible range), that lead to a linear dispersion of about 2.1 nm/mm or 1.05 nm/mm, respectively. The choice of the grating was mainly dictated by the optimization of signal intensity – the 1200 lines/mm grating was used for the detection of Fe, while the 2400 lines/mm was used for the detection of Pb. The spectrometer was coupled to an ICCD detector (Andor iStar, DH720-25-H-05) containing 1024 × 256 pixels of dimensions 26 μm × 26 μm. The width of the acquisition spectral window was about 22 nm for the 1200 lines/mm, and 11 nm for the 2400 lines/mm. The resolution was basically limited by the fibre core diameter since the spectrometer entrance slit width was larger than the single-fibre diameter.

Regarding the acquisition temporal parameters, the integration delay was set to $t = \Delta t_{IP} - 150$ ns, where Δt_{IP} is the inter-pulse delay (delay between the ablation and excitation pulses), and the gate width was $\Delta t = 400$ ns. Considering that the fluorescence decay time for each excitation/fluorescence scheme probed is around a few tens of ns (a few times $1/A_{mn}$, where A_{mn} is the spontaneous transition rate from excited level m to metastable level n), these settings allowed the recording of the fluorescence signal in its entirety, avoiding any signal loss due to possible jitter or insertion delays. A long wave pass filter was positioned at the input of the spectrometer to filter the scattered laser radiation due to the presence of the OPO pulse during the acquisition gate, thus reducing the noise level due to stray light in the acquired spectra.

To improve the shot-to-shot reproducibility of the measurements (issue of persistent concern while applying LIBS to

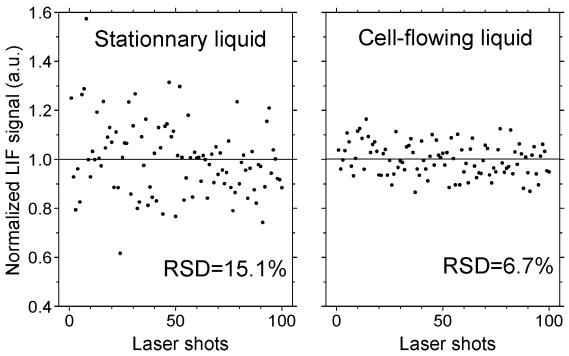

Fig. 2 LIBS-LIF signal for the detection of Pb atoms as a function of the number of laser shots in the case of a stationary liquid (left) and a flow cell (right).

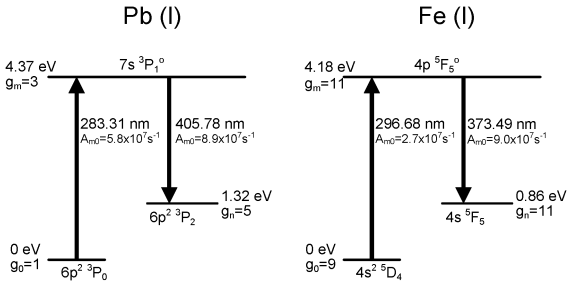

Fig. 3 Simplified energy level diagram for Pb and Fe. The laser excited and fluorescence wavelengths are also shown, as well as spontaneous emission rates A_{mn} and level multiplicities g_m.

liquids), an in-house sample cell in Teflon was developed. A continuous flow through this cell was achieved by means of a peristaltic pump (Masterflex) and a tubing system (Chemdurance −17 mm diameter). The total liquid solution volume in the cell was about 125 mL while the flow rate through the cell was set to 130 mL/min, to maintain a good stability of the flow. This setup was used to detect small amounts of Pb and Fe in weak acid aqueous solutions (4% HNO_3) in the concentration range from 300 ppb to 500 ppm. These solutions were home-prepared by successive dilutions of 1000 ppm atomic absorption certified standards (SCP science). In this study, from 30 (Section 3) to 100 (Section 4) spectra were acquired for each solution, in order to get into account of experimental fluctuations, mainly in the ablation laser energy and in light collection.

As shown in Fig. 2, under optimal operating conditions in terms of pumping speed, flow rate and laser repetition rate a shot-to-shot relative standard deviation (RSD) as low as 6.7% was achieved, for series of 100 shots, whereas this value was 15.1% for a stationary liquid. The series-to-series RSD (comparison of the mean LIBS-LIF signal obtained for 10 successive series of 100 shots) went down to about 2%, which corresponds to a fairly high level of reproducibility when compared to other works performed on liquids at comparable or lower repetition rates. For instance, a value of 4.5% was achieved for 10 series of 300 shots at a repetition rate of 5 Hz in Ref. 40, while a value of 5% was determined for 10 series of 100 shots at a repetition rate of 1 Hz in Ref. 41. Also, it is worth mentioning that no data treatment aiming to the removal of outliers was carried out to reach such a good reproducibility in the measurements.

C Results and discussion

C.1 Laser-induced fluorescence for the detection of Pb and Fe atoms

Fig. 3 illustrates the excitation/fluorescence schemes investigated in this paper for Pb and Fe. Both of these three-level excitation/fluorescence schemes belong to the thallium-like type and give rise, in particular, to a Stokes direct-line fluorescence.[42]

The neutral Pb atoms were excited by the OPO laser radiation tuned at 283.31 nm, from the ground state $6p_2\ ^3P_0$ (at 0 eV) to the $7s\ ^3P_1^0$ state (at 4.37 eV), leading to a radiative de-excitation from this state to the radiatively metastable $6p_2\ ^3P_2$ state (at 1.32 eV), emitting the direct-line fluorescence at 405.78 nm. Among all LIF schemes for Pb, this one is expected to be the most efficient, in terms of excitation and fluorescence, based on the high values of spontaneous emission rates (A_{mn}, A_{m0}) and a favourable branching ratio of 0.49 for the 405.78 nm line.

For Fe, the excitation wavelength was tuned to 296.68 nm, which pumped Fe neutral atoms from the ground state $4s^2\ 5D_4$ (at 0 eV) to the $4p\ 5F_5^0$ state (at 4.17 eV), inducing the direct-line fluorescence at 373.49 nm, from this state to the $4s\ 5F_5$ state (at 0.86 eV) that is radiatively metastable. As for Pb, this LIF scheme is also predicted to be very efficient with a 373.49-nm line branching ratio of 0.77. However, since the $4p\ 5F_5^0$ state lies in a region of closely-spaced energy levels, thermally-activated transitions from the pumped level to nearby levels followed by de-excitation *via* other channels are expected. Indeed, several emission lines, corresponding to transitions originating from levels located in the 4.09–4.34 eV region (essentially belonging to the $5D_J^\circ$, $5F_J^\circ$ and $3P_J^\circ$ configurations), were observed in the acquired spectra. Nevertheless, the energy contained in those transitions does not seem to exceed more than 10% to 20% of the energy emitted in the main fluorescence channel.

Fig. 4 shows the LIF signal intensities obtained for the Pb(I) 405.78 nm and Fe(I) 373.49 nm analytical lines as a function of

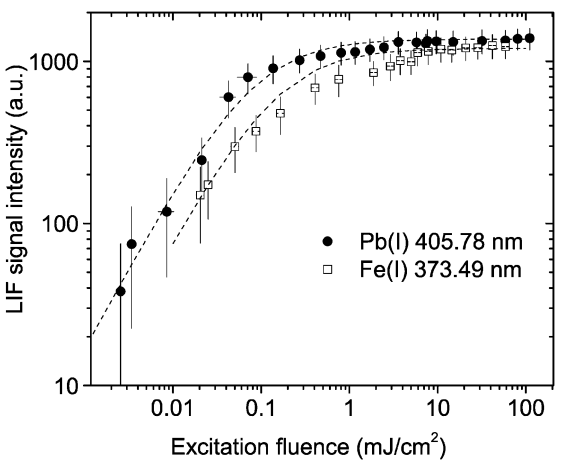

Fig. 4 LIF signal intensity for the Pb(I) 405.78 nm and Fe(I) 373.49 nm fluorescence lines as a function of the excitation fluence. The results were obtained by averaging over 30 laser shots.

the excitation fluence. Each sample contained 10 ppm of the trace element under investigation. Such a low concentration was used to avoid self-absorption of the induced fluorescence radiation.[43]

Based on the results discussed in the next section regarding the optimization of the LIF signal for our setup, the interpulse delay was set to 11 μs while the ablation fluence was 18 J/cm^2 for Pb and Fe. The excitation energy was varied from 0.1 to 2600 μJ, which corresponds to a fluence ranging from 0.004 to 110 mJ/cm^2.

In Fig. 4, two different regimes can be identified for both elements, as observed in typical LIF measurements.[43] For weak excitation fluences, *i.e.*, less than 0.1 mJ/cm^2, the LIF signal grows linearly when increasing the excitation fluence. Even if data for low excitation fluences are relatively scarce, this behaviour appears quite clearly, especially in the case of Pb. Indeed, the number of atoms excited to the upper level of the excitation/fluorescence scheme is directly proportional to the number of incoming photons from the OPO beam. As the excitation fluence further increases, the LIF signals depart from linearity and reach a plateau corresponding to the optical saturation regime. The maximum values of both LIF signals for Pb and Fe are almost identical, so similar LoDs are expected when using LIBS-LIF for these elements.

Assuming that a steady state prevails, the LIF signal as a function of the excitation fluence is given by the following expression:[34]

$$I_{fluo} = I_{fluo}^{max} \cdot \frac{F_{exc}}{F_{exc} + F_{exc}^{sat}} \quad (1)$$

where I_{fluo} is the intensity of the LIF signal, I_{fluo}^{max} is the LIF intensity at saturation, F_{exc} is the excitation fluence, and F_{exc}^{sat} is the saturation parameter defined by the excitation fluence for which the LIF signal reaches 50% of its saturation value. By fitting Eq. (1) to the measurements, we obtained $F_{exc}^{sat} = 0.08$ and 0.15 mJ/cm^2 for Pb and Fe, respectively. The corresponding fits are shown in Fig. 4. For Pb, the fit closely describes the behaviour of the LIF signal, whereas more significant deviation appears for Fe, especially near saturation. The discrepancies between the experimental data and the theoretical fits could be mainly attributed to two effects. Indeed, Eq. (1) should hold only when a steady-state regime is reached during the pumping process.[42] This condition might not be verified with the 7 ns pulse used in our experiments. In addition, spatial inhomogeneity of the excitation beam might lead to notably different absorption efficiencies from the center to the beam wings. This could result in a shift of the saturation parameter and departures from Eq. (1) near saturation.[44] In the case of Fe, the energy lost through thermal activation, which, as mentioned earlier, decreases when increasing the excitation fluence, could also contribute to the departure from Eq. (1). In principle, both saturation parameters for Pb and Fe can be calculated by solving the rate equations for a "thallium-like" three-level LIF scheme.[43] Unfortunately values of the excitation and de-excitation rates for the collisionnally induced transitions between levels are not known in our specific conditions. When considering only radiative transitions and a Gaussian laser pulse, both saturation parameters are at least one order of magnitude higher than our experimental values. Further work is required for a proper calculation of the saturation parameters, which is clearly beyond the scope of this paper mainly focused on analytical performances.

In the following, the measurements were carried out under optical saturation, *i.e.*, with excitation fluences above a few tens of mJ/cm^2, to maximize the LIF signal and also limit its variations due to excitation energy fluctuations.

C.2 Optimal plasma conditions for efficient LIF operation

Fig. 5 shows the the signal-to-noise ratio for the Pb(I) 405.78 nm and Fe(I) 373.49 nm lines as a function of the interpulse delay. The results are shown for several ablation fluences ranging from 4.1 to 19.4 J/cm^2. The same behaviour is observed for both elements. For a given ablation fluence, the LIF signal first increases with the interpulse delay until it reaches a maximum, for an interpulse delay value which increases with the ablation fluence.

The observed trend relies partly on the number of atoms present in the ground state when the excitation beam is injected in the plasma volume and partly on the collisional de-excitation rate of the states excited by the OPO laser. For short delays, the plasma temperature is relatively high so that different excitation and ionization stages still co-exist in the plasma, resulting in a relatively weak amount of neutral atoms in the ground state. In

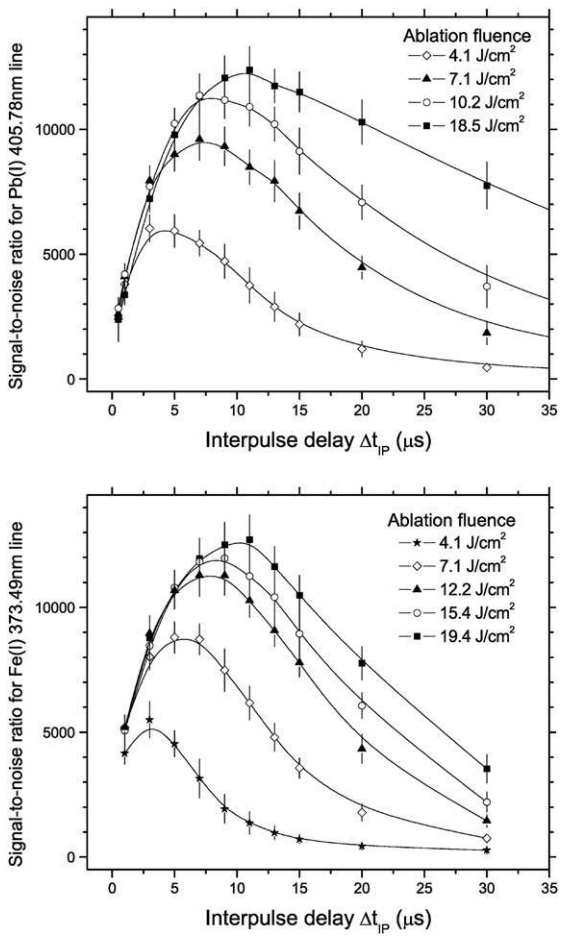

Fig. 5 Signal-to-noise ratio for the Pb(I) 405.78 nm (top graph) and Fe(I) 373.5 nm (bottom graph) lines as a function of the interpulse delay for ablation fluences ranging from 4.1 to 19.4 J/cm^2. Each solution contained 100 ppm of Pb or Fe, and the LIF signals were averaged over 30 laser shots.

addition, the collisional de-excitation rate is higher at higher temperature so that the fluorescence signal is lower. Generally, in LIBS, the lines emitted by singly ionized atoms are still visible out to the μs timescale. Increasing the interpulse delay allows the plasma to cool down until a temperature enabling to have a large fraction of neutral atoms in the ground state is reached. This results in an enhanced LIF signal. For both elements, the optimal interpulse delay is about $\Delta t_{IP} = 11$ μs for the highest ablation fluence used here.

To verify this assumption, we measured the electron temperature of the plasma at different times. The results are shown in Fig. 6 for three ablation fluences between 10 and 20 J/cm^2. A solution containing 1000 ppm of Fe was used for these measurements and the temperature was determined using Boltzmann plots based on a set of nine Fe I lines between 370 and 377 nm.[45] We checked that no self-absorption occurred for these lines by following the procedure described by Miller and Debroy.[46]

One observes that for the highest ablation fluence, 19.4 J/cm^2, the electron temperature varies from 8500 K just 1 μs after the ablation pulse to about 4500 K after 10 μs. As a first estimate, assuming that the Pb excited states follow a Boltzmann distribution, about 30% and 70% of the atoms lie in the ground state for these two temperatures, respectively. A similar calculation performed for Fe gives about 20% and 35% instead. These estimates are consistent with the general trends observed in Fig. 5 before the maximum. For the lower ablation fluences (15.3 and 10.2 J/cm^2), the weaker intensity of the Fe lines did not allow to follow the evolution of the temperature out to late times. Nevertheless, it is clear from Fig. 6 that the temperature is lower for a lower fluence at a given time and that low temperatures are reached earlier when compared to the 19.4 J/cm^2 case. This likely explains the shift in the optimal operating conditions observed for each element in Fig. 5.

This explanation alone would however involve a saturation of the LIF signal with the interpulse delay. The decrease observed in Fig. 5 for longer delays likely results from both the late-evolution of the plasma (end of the atomization process and subsequent atom recombination) and the optical arrangement of the experimental setup. Indeed, as the plasma cools down, it expands until its spatial extension exceeds that of the OPO excitation beam. Beyond that point, an increasing number of atoms stand outside the plasma and excitation beam overlap region, and do not contribute to the signal. Moreover, the characteristics of the optical parts used in the setup (the collection lens focal length, and the optical fiber size and acceptance cone), as well as their specific arrangement (plasma-to-collection lens and collection lens-to-fiber distance) allows only a 2.5-mm diameter object to be imaged properly at the entrance of the fiber. This experimental limitation also contributes to the lowering of the LIF signal for high interpulse delay values, hence spatially extended plasmas.

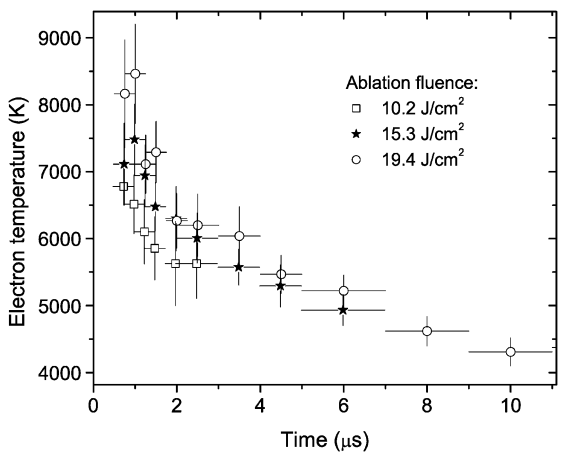

Fig. 6 Time-resolved evolution of the electron temperature of the plasma for three ablation fluences (10.2, 15.3 and 19.4 J/cm^2). The results were obtained using a 1000 ppm Fe solution. The intensities were averaged over 30 laser shots while horizontal bars indicate the gate width of Fe I lines acquisition.

Clearly, the optimal operating conditions, for which the LIF signal can be maximized for the detection of each trace element, result from a compromise between the ablation fluence (high enough to provide a large number of atoms to be probed), the interpulse delay (long enough for the plasma to reach a temperature allowing the ground state of atoms to be populated) and the optical arrangement of the experimental setup (limiting factor for the spatial extension of the plasma and the region probed). As these optimal conditions strongly depend on the experimental design, different results can be expected for different setups. Indeed, even if a similar overall behaviour was found in other works, different specific optimal parameters were deduced. For instance, in Ref. 32, the LIF signal was maximized for an interpulse delay of about 6 μs for an ablation energy of 25 mJ (information about the ablation spot diameter was not given), whereas in Ref. 33 the optimum was obtained for a delay of 800 ns for an ablation energy of 260 μJ (corresponding to a fluence around 330 J/cm^2). Similar trends were also observed on solid or aerosol samples, for instance for the detection of Si in steels,[24] or Pb in lead nitrate aerosols[35] and in brass samples.[47]

D Calibration curves for LIBS-LIF and LIBS

In this section the LoDs obtained using LIBS-LIF with the optimized parameters discussed in the previous section, are compared with those obtained using conventional LIBS. For that purpose, we used a set of known concentrations from 0.3 to 250 ppm of Pb or Fe for LIBS-LIF. For LIBS we also used additional samples containing 500 ppm of Pb or Fe.

Fig. 7 shows the signal-to-noise ratio as a function of the Pb and Fe concentration using the LIBS-LIF and LIBS techniques. For LIBS-LIF the Pb(I) 405.78 nm and Fe(I) 373.49 nm lines were used for detection (see Fig. 3), while the Pb(I) 405.78 nm and Fe(I) 358.12 nm were used for LIBS. Spectra obtained using LIBS-LIF for the lowest concentration (300 ppb) are also shown in the insets of Fig. 7. For LIBS measurements, the acquisition delay and gate width were $t = 0.5$ μs and $\Delta t = 15$ μs, respectively, and the spectrometer entrance slit width was 100 μm. The LoDs were then calculated according to the IUPAC 3σ-convention, where σ is the dark current noise that was evaluated on a spectral region free of lines.

For both techniques we averaged the signal-to-noise ratio over 100 laser shots. The values of the LoD achieved with LIBS-LIF were 39 ppb for the detection of Pb, and 65 ppb for Fe. With conventional LIBS, comparatively, we were only able to reach

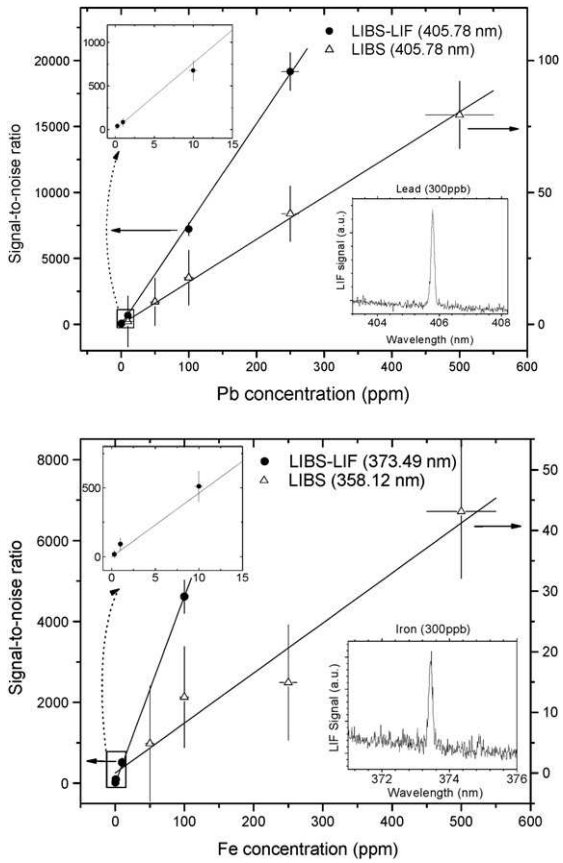

Fig. 7 Signal-to-noise ratio as a function of the concentration for Pb (top graph) and Fe (bottom graph) obtained by the LIBS and LIBS-LIF techniques. Insets on the top-left show the behaviour of the LIBS-LIF calibration curves for low-concentration samples, and insets on the bottom-right represent the LIBS-LIF spectra obtained for a 300 ppb concentration. The results were obtained by averaging over 100 laser shots.

LoD values of 19 ppm for Pb and 37 ppm for Fe. In both cases, the enhancement in the analytical performance is around 2–3 orders of magnitude (490 and 570 times for Pb and Fe, respectively).

Although evaluating the ablation rate in liquids is a complex issue (no quantitative work could be found in the literature), an upper-bound value of 140 ng can be estimated for an ablation fluence of 19 J/cm^2 and a 500 μm spot diameter. This value was obtained assuming that all the laser energy is used to vaporize water, dissociate the water molecules, and ionize once H and O. The absolute LoDs for Pb and Fe can thus be estimated to be about 65 fg and 30 fg, respectively, *i.e.*, about 2.5×10^8 atoms.

In terms of signal-to-noise ratio, the significant enhancement of the LoD brought by the LIBS-LIF technique is mainly due to: 1) the larger amount of excited atoms, and 2) the lower noise level allowed by the short acquisition gate of the analytical signal and the absence of the early plasma continuum emission. Indeed, typical noise level was about 1 ICCD count in our LIBS-LIF measurements ($\Delta t = 0.4$ μs), whereas its value was about 80 counts for LIBS ($\Delta t = 15$ μs). Another advantage of LIBS-LIF is the better linearity characterizing the calibration curves. Indeed, the R^2 coefficients of the linear fits were as high as 0.99 for both elements while those obtained with LIBS were 0.98 for Pb and 0.92 for Fe. In addition the linearity range of the calibration curve should be greater when using LIBS-LIF. Indeed, during the acquisition gate, self-absorption is expected to be weaker since the number density of the species to detect is lower when compared to LIBS. Finally, the selective nature of LIBS-LIF generally prevents from any spectral interference between the analytical line and other lines which might represent a strong limitation when using LIBS.

Similar studies on LIBS-LIF in liquids have been performed by other groups. In a μ-LIBS framework, Godwal *et al.* demonstrated an 18-times improvement of the LoD from LIBS to LIBS-LIF, with values of, respectively, 75 ppm and 4.3 ppm averaging over 100 laser shots.[33] In the case of Fe, Nakane *et al.* estimated a LoD in the range of 10 ppb with the same detection scheme as the one used in this work but without any mention of the number of acquisition shots.[32] A general conclusion that can be drawn from our work and the literature points towards a maximum achievable enhancement of the LoD around 3 orders of magnitude using LIBS-LIF compared to LIBS, considering both liquids and solids.

E Conclusion

In this paper, we investigated the detection of traces of metallic impurities in liquid acid solutions using LIBS combined with LIF. The influence of the main experimental parameters on the LIF signal was studied and operating conditions were determined to optimize the LoD. For our specific LIBS-LIF experimental arrangement, using the 266 nm fourth-harmonic of a Q-switched Nd:YAG laser for the ablation, the best signal-to-noise ratio was achieved for the highest ablation energy available in our setup (corresponding to a fluence of about 19 J/cm^2 for a laser spot diameter of 500 μm), an interpulse delay of about 11 μs and an excitation fluence of a few mJ/cm^2. The optimum found in the LIF signal as a function of the interpulse delay was interpreted in terms of plasma temperature, populations of quantum states and collisional de-excitation rate. The best LoDs obtained were 39 ppb and 65 ppb for Pb and Fe solutions, respectively, accumulating over 100 shots. These values are 2 to 3 orders of magnitude smaller than the ones obtained with LIBS in the best conditions using the same experimental setup. The problem of reproducibility of the LIBS-LIF measurements, which is of great importance when analyzing liquids, has also been successfully tackled using a flow cell. A relative standard deviation as low as 6.7% for series of 100 laser shots was achieved for an ablation laser repetition rate of 0.7 Hz.

Despite the higher setup complexity occasioned by the use of a second laser pulse, the LIBS-LIF technique appears as a promising tool for fast, remote, on-line and real-time applications requiring sub-ppm trace detection levels. However, starting from our laboratory setup, additional technical developments may be necessary in order to meet the requirements of specific analytical applications, as, for instance, reducing the sample volume, hence the flow-cell dimensions. In this frame, other improvements may also be worth considering. Among them, and due to the mono-elemental nature of the technique, the use of an interference filter followed by a higher sensitivity photomultiplier tube, instead of the usual spectrometer and ICCD camera combination is likely to further enhance the performances of the technique.

Acknowledgements

The authors would like to acknowledge Pierre-Philippe Bérubé at the IMI-NRC for his participation to the sample cell design. This work was financially supported by the Natural Science and Engineering Research Council of Canada (NSERC).

References

1 L. St-Onge, E. Kwong, M. Sabsabi and E. B. Vadas, Quantitative analysis of pharmaceutical products by laser-induced breakdown spectroscopy, *Spectrochim. Acta, Part B*, 2002, **57**, 1131–1140.
2 J. J. Bolger, Semi-quantitative laser-induced breakdown spectroscopy for analysis of mineral drill core, *Appl. Spectrosc.*, 2000, **54**, 181–189.
3 O. Samek, D. C. S. Beddows, J. Kaiser, S. V. Kukhlevsky, M. Liska, H. H. Telle and J. Young, Application of laser-induced breakdown spectroscopy to in situ analysis of liquid samples, *Opt. Eng.*, 2000, **39**, 2248–2262.
4 D. A. Cremers, L. J. Radziemski and T. R. Loree, Spectrochemical analysis of liquids using the laser spark, *Appl. Spectrosc.*, 1984, **38**, 721.
5 J. R. Wachter and D. A. Cremers, Determination of uranium in solution using laser-induced breakdown spectroscopy, *Appl. Spectrosc.*, 1987, **41**, 1042.
6 R. Knopp, F. J. Scherbaum and J. I. Kim, Laser induced breakdown spectroscopy (LIBS) as an analytical tool for the detection of metal ions in aqueous solutions, *Fresenius' J. Anal. Chem.*, 1996, **355**, 16.
7 K. Meissner, T. Lippert, A. Wokaun and D. Guenther, Analysis of trace metals in comparison of laser-induced breakdown spectroscopy with LA-ICP-MS, *Thin Solid Films*, 2004, **453–454**, 316–322.
8 P. Fichet, M. Tabarant, B. Sallé and C. Gauthier, Comparisons between LIBS and ICP/OES, *Anal. Bioanal. Chem.*, 2006, **385**, 338–344.
9 D. A. Cremers and L. J. Radziemski, *Handbook of laser-induced breakdown spectrscopy*, John Wiley & Sons, Chichester, 2006.
10 A. Miziolek, *Laser-induced breakdown spectroscopy (LIBS): fundamentals and applications*, Cambridge University Press, Cambridge UK, New York, 2006.
11 G. Asimellis, S. Hamilton, A. Giannoudakos and M. Kompitsas, Controlled inert gas environment for enhanced chlorine and fluorine detection in the visible and near-infrared by laser-induced breakdown spectroscopy, *Spectrochim. Acta, Part B*, 2005, **60**, 1132–1139.
12 L. St-Onge, V. Detalle and M. Sabsabi, Enhanced laser-induced breakdown spectroscopy using the combination of fourth-harmonic and fundamental Nd:YAG laser pulses, *Spectrochim. Acta, Part B*, 2002, **57**, 121–135.
13 B. Le Drogoff, J. Margot, F. Vidal, S. Laville, M. Chaker, M. Sabsabi, T. W. Johnston and O. Barthélemy, Influence of the laser pulse duration on laser-produced plasma properties, *Plasma Sources Sci. Technol.*, 2004, **13**, 223–230.
14 S. Laville, F. Vidal, T. W. Johnston, M. Chaker, B. Le Drogoff, O. Barthelemy, J. Margot and M. Sabsabi, Modeling the time evolution of laser-induced plasmas for various pulse durations and fluences, *Phys. Plasmas*, 2004, **11**, 2182–2190.
15 B. Le Drogoff, M. Chaker, J. Margot, M. Sabsabi, O. Barthélemy, T. W. Johnston, S. Laville and F. Vidal, Influence of the laser pulse duration on spectrochemical analysis of solids by laser-induced plasma spectroscopy, *Appl. Spectrosc.*, 2004, **58**, 122–129.
16 O. Barthélemy, J. Margot, M. Chaker, M. Sabsabi, F. Vidal, T. W. Johnston, S. Laville and B. Le Drogoff, Influence of the laser parameters on the space and time characteristics of an aluminum laser-induced plasma, *Spectrochim. Acta, Part B*, 2005, **60**, 905–914.
17 Y. Lee, S. P. Sawan, T. L. Thiem, Y. Teng and J. Sneddon, Interaction of a laser beam with metals. Part II: Space-resolved studies of laser-ablated plasma emission, *Appl. Spectrosc.*, 1992, **46**, 436–441.
18 I. S. Borthwick, K. W. D. Ledingham and R. P. Singhal, Resonant laser ablation - a novel surface analytic technique, *Spectrochim. Acta,Part B*, 1992, **47**, 1259–1265.
19 L. St-Onge, M. Sabsabi and P. Cielo, Analysis of solids using laser-induced plasma spectroscopy in double-pulse mode, *Spectrochim. Acta, Part B*, 1998, **53**, 407–415.
20 J. Scaffidi, J. Pender, W. Pearman, S. R. Goode, B. W. Colston, J. C. Carter and S. M. Angel, Dual-pulse laser-induced breakdown spectroscopy with the combinations of femtosecond and nanosecond pulses, *Appl. Opt.*, 2003, **42**, 6099–6106.
21 P. Stchur, K. X. Yang, Xi, E. Hou, T. Sun and R. G. Michel, Laser excited atomic fluorescence spectrometry - a review, *Spectrochim. Acta, Part B*, 2001, **56**, 1565–1592.
22 O. Samek, M. Liska, J. Kaiser, V. Krzyzanek, D. C. S. Beddows, A. Belenkevitch, G. W. Morris and H. H. Telle, Laser ablation for mineral analysis in the human body: integration of LIFS with LIBS, *Proc. SPIE*, 1999, **3570**, 263.
23 B. W. Smith, I. B. Gornushkin, L. A. King and J. D. Winefordner, A laser ablation–atomic fluorescence technique for isotopically selective determination of lithium in solids, *Spectrochim. Acta, Part B*, 1998, **53**, 1131–1138.
24 W. Sdorra, A. Quentmeier and K. Niemax, Basic investigations for laser microanalysis: II. Laser-induced fluorescence in laser-produced sample plumes, *Microchim. Acta*, 1989, **98**, 201–218.
25 J. B. Gornushkin, J. E. Kim, B. W. Smith, S. A. Baker and J. D. Winefordner, Determination of cobalt in soil, steel, and graphite using excited-state laser fluorescence induced in a laser spark, *Appl. Spectrosc.*, 1997, **51**, 1055–1059.
26 F. Hilbk-Kortenbruck, R. Noll, P. Wintjens, H. Falk and C. Becker, Analysis of heavy metals in soils using laser-induced breakdown spectrometry combined with laser-induced fluorescence, *Spectrochim. Acta, Part B*, 2001, **56**, 933–945.
27 S. C. Snyder, J. D. Grandy and J. K. Partin, *An investigation of laser-induced breakdown spectroscopy augmented by laser-induced fluorescence, ICALEO'98*: Laser Materials Processing Conference, Orlando, 1998, 254–261.
28 I. Gormushkin, S. Baker, B. Smith and J. Winefordner, Determination of lead in metallic reference materials by laser ablation combined with laser excited atomic fluorescence, *Spectrochim. Acta, Part B*, 1997, **52**, 1653–1662.
29 B. W. Smith, A. Quentmeier, M. Bolshov and K. Niemax, Measurement of uranium isotope ratios in solid samples using laser ablation and diode laser-excited atomic fluorescence spectrometry, *Spectrochim. Acta, Part B*, 1999, **54**, 943–958.
30 H. H. Telle, D. C. S. Beddows, G. W. Morris and O. Samek, Sensitive and selective spectrochemical analysis of metallic samples: the combination of laser-induced breakdown spectroscopy and laser-induced fluorescence spectroscopy, *Spectrochim. Acta, Part B*, 2001, **56**, 947–960.
31 S. Koch, W. Garen, W. Neu and R. Reuter, Resonance fluorescence spectroscopy in laser-induced cavitation bubbles, *Anal. Bioanal. Chem.*, 2006, **385**, 312–315.
32 M. Nakane, A. Kuwako, K. Nishizawa, H. Kimura, C. Konagai and T. Okamura, Analysis of trace metal elements in water using laser-induced fluorescence for laser-breakdown spectroscopy, *Proc. SPIE*, 2000, **3935**, 122–131.
33 Y. Godwal, S. Lui, M. Taschuk, Y. Tsui and R. Fedosejevs, Determination of lead in water using laser ablation–laser induced fluorescence, *Spectrochim. Acta, Part B*, 2007, **62**, 1443–1447.
34 S. L. Lui, Y. Godwal, M. T. Taschuk, Y. Y. Tsui and R. Fedosejevs, Detection of lead in water using laser-induced breakdown spectroscopy and laser-induced fluorescence, *Anal. Chem.*, 2008, **80**, 1995–2000.
35 R. E. Neuhauser, U. Panne, R. Niessner, G. A. Petrucci, P. Cavalli and N. Omenetto, On-line and in-situ detection of lead aerosols by plasma-spectroscopy and laser-excited atomic fluorescence spectroscopy, *Anal. Chim. Acta*, 1997, **346**, 37–48.
36 F. Y. Yueh, R. C. Sharma, J. P. Singh, H. Zhang and W. A. Spencer, evaluation of the potential application of laser-induced breakdown spectroscopy for detection of trace element in liquid, *J. Air Waste Manage. Assoc.*, 2002, **52**, 1307–1315.
37 R. L. Vander Wal, T. M. Ticich, J. R. West Jr. and P. A. Householder, Trace metal detection by laser-induced breakdown spectroscopy, *Appl. Spectrosc.*, 1999, **53**, 1226–1236.
38 J. Schou, A. Matei, K. Rodrigo and M. Dinescu, Laser-induced plasma from pure and doped water-ice at high fluence by ultraviolet and infrared radiation, *Proc. SPIE*, 2008, **7005**, 70050X.
39 J. Noack and A. Vogel, Laser-induced plasma formation in water at nanosecond to femtosecond time scales: calculation of thresholds, absorption coefficients, and energy density, *IEEE J. Quantum Electron.*, 1999, **35**, 1156–1167.
40 Z. Chen, H. Li, M. Liu and R. Li, Fast and sensitive trace metal analysis in aqueous solutions by laser-induced breakdown spectroscopy using wood slice substrates, *Spectrochim. Acta, Part B*, 2008, **63**, 64–68.

41 G. Arca, A. Ciucci, V. Palleschi, S. Rastelli and E. Tognoni, Trace element analysis in water by the laser-induced breakdown spectroscopy technique, *Appl. Spectrosc.*, 1997, **51**, 1102–1105.
42 N. Omenetto, *Analytical laser spectrometry*, John Wiley & Sons, New York, 1979.
43 D. R. Olivares and G. M. Hietfje, Saturation of energy levels in analytical atomic fluorescence spectrometry – I. Theory, Spectrochim, *Spectrochim. Acta, Part B*, 1978, **33**, 79–98.
44 J. W. Daily, Saturation of fluorescence in flames with a Gaussian laser beam, *Appl. Opt.*, 1978, **17**, 225–229.
45 M. Sabsabi and P. Cielo, Quantitative analysis of aluminum alloys by laser-induced breakdown spectroscopy and plasma characterization, *Appl. Spectrosc.*, 1995, **49**, 499–507.
46 R. Miller and T. Debroy, Energy absorption by metal-vapor-dominated plasma during carbon dioxide laser welding of steels, *J. Appl. Phys.*, 1990, **68**, 2045–2050.
47 S. Laville, C. Goueguel, H. Loudyi, F. Vidal, M. Chaker and M. Sabsabi, Laser induced fluorescence detection of lead atoms in a laser induced plasma: an experimental analytical optimization study, *Spectrochim. Acta, Part B*, 2009, **64**, 347–353.

